



# Synthesis and characterization of nano zinc oxide/zinc chloride–activated carbon composite based on date palm fronds: adsorption of methylene blue

Laila M. Alshandoudi<sup>1</sup> · Said R. Alkindi<sup>1</sup> · Tariq Y. Alhatmi<sup>1</sup> · Asaad F. Hassan<sup>2</sup>

Received: 10 November 2022 / Revised: 30 December 2022 / Accepted: 14 January 2023 / Published online: 25 January 2023  
© The Author(s), under exclusive licence to Springer-Verlag GmbH Germany, part of Springer Nature 2023

## Abstract

Zinc chloride–activated carbon (AC) and nano zinc oxide/activated carbon composite (NZAC) as solid adsorbents were synthesized from date palm fronds (DPF) as a green material of activated carbon, while zinc oxide nanoparticles (NZ) were prepared in the presence of polyethylene glycol as capping agent. All the prepared solid adsorbents were investigated by several characterization techniques such as thermogravimetric analysis (TGA), nitrogen adsorption/desorption isotherm, Fourier transform infrared spectroscopy (FTIR), pH of point of zero charges ( $\text{pH}_{\text{PZC}}$ ), scanning electron microscopy (SEM), and transmission electron microscope (TEM). The NZAC sample had the highest total pore volume ( $0.960 \text{ cm}^3/\text{g}$ ), specific surface area ( $2085.47 \text{ m}^2/\text{g}$ ), and with  $\text{pH}_{\text{PZC}}$  of 7.8. Adsorption of methylene blue was tested by Langmuir, Freundlich, and Temkin adsorption isotherms. NZAC had the highest Langmuir adsorption capacity ( $456.62 \text{ mg/g}$ ) at  $40^\circ\text{C}$  with a dimensionless separation factor ( $R_L$ ) of 0.030. MB adsorption matched well with pseudo-second-order and Elovich kinetic models. The entropy, free energy, and heat changes for MB adsorption onto NZAC were found to be  $0.0243 \text{ (kJ/mol. K)}$ ,  $-3.5589 \text{ (kJ/mol)}$ , and  $3.561 \text{ (kJ/mol)}$ , respectively. Thermodynamic analysis demonstrated that the adsorption process of MB is favorable, spontaneous, physisorption, and endothermic. Desorption studies showed that HCl ( $0.01 \text{ mol/L}$ ) achieved the higher desorption percent (87%) compared with the other eluents.

**Keywords** Palm fronds · Composite · Methylene blue · Adsorption · Isotherms · Kinetics

## 1 Introduction

Water contamination has attracted the public attention and emerged as one of the most important issues in the last several decades because of the world's fast industrialization. The release of pollutants from many sectors generates significant difficulties for aquatic and human life due to their toxic effects even at low concentrations [1]. The textile industry includes many processes such as printing, dyeing, and bleaching which lead to discharging of many pollutants as wastes in natural streams [2]. It was noted that

annually, more than  $7 \times 10^5$  tones of dyes are produced. This wastewater contains large amounts of high concentrations of toxic organic dyes [3]. Methylene blue dye is the most dispersed dye in water and is linked to several illnesses and symptoms, including nausea, vomiting, irritated mouth and throat, elevated heart rate, jaundice, tissue necrosis, anemia, and quadriplegia. So, the wastewater contaminated with MB dye should be properly treated [4]. Also, due to organic dyes' aromatic complex structure, non-biodegradable properties, and recalcitrant nature, the formation of byproducts that are more toxic than the dye molecule starts to kill biological organisms and conventional biological methods for the treatment of organic dyes are ineffective [5]. Several physical and chemical methods such as coagulation [6], membrane filtration [7], photocatalytic degradation [8], ion exchange [9], electrochemical oxidation [10], ozonation [11], flocculation, reduction, and adsorption are used for the treatment of dyes. Among all the other treatment options, adsorption is a promising technique for the elimination of dyes owing to its design simplicity, reusability, and flexibility efficiency.

✉ Asaad F. Hassan  
asmz68@sci.dmu.edu.eg

<sup>1</sup> Science Department, Al Rustaq College of Education, University of Technology and Applied Sciences, Al Rustaq, Sultanate of Oman

<sup>2</sup> Chemistry Department, Faculty of Science, Damanhour University, Damanhour, Egypt

Different materials including zeolite granules [12], chitosan [13], biochar [14], silica-based materials [15], ionic liquid – graphene oxide sponge [16], metal–organic frameworks [17], and polymeric materials [18] have been investigated for the adsorption of dyes. Some of these adsorbents can eliminate contaminants from water but suffer from some drawbacks like high cost, low efficiency, and poor reusability. Activated carbon is the most preferred adsorbent for the removal of dyes because of its excellent ability in the adsorption process regardless of the restricted use of activated carbon because of its high cost. Both physical and chemical activation techniques are used to prepare activated carbon, but chemical activation has a number of advantages over physical activation, such as the fact that it only requires one step, operates at lower temperatures, typically has a better impact on pore growth, uses less energy, and yields high carbon yields. For the creation of activated carbon, many researchers have adopted the chemical activation approach [19]. The biomasses are soaked with a variety of chemical-activating agents during chemical activation, including  $\text{ZnCl}_2$  [20],  $\text{KOH}$  [21],  $\text{H}_2\text{SO}_4$  [22],  $\text{HCl}$  [23],  $\text{H}_3\text{PO}_4$  [24], and  $\text{H}_2\text{O}_2$  [25].

The adsorption onto low-cost adsorbents including byproducts from industry or agriculture and natural materials is considered one of the most highly interesting processes due to its ease of implementation and low cost. The utilization of inexpensive agricultural byproducts has attracted more attention in recent years. Agricultural wastes like different kinds of shells (coconut, palm tree, walnut, almond, durian, pistachio, acorn, groundnut, hazelnut), stalks (rice, cotton, grape), leaves (spent tea, dry or dead), straws (wheat, barley), peels (cassava), seeds (Jajoba, pomegranate), husks (wheat, coconut, *Jatropha*, rice), and even stones (olive, date) have been reported for the activated carbon production [26]. Among these wastes, date palm trees represent the first crop in the Sultanate of Oman with 325 types of dates with total fruits cultivated area ~62 thousand acres, more than 9.1 million trees to produce about 374 thousand tons of date annually. The huge quantities of palm tree waste encourage us to use it as a precursor for the production of valuable activated carbon from date palm fronds which are considered a pollutant especially when transferred into landfill.

In the field of material science, researchers created various nano-sized materials of less than 100 nm using chemical, biological, and physical methods. The high activity of nanoparticles is caused by their higher surface area to volume ratio, and their activities are exploited in various fields [27]. To remove dyes from aqueous solutions, different metal oxides such as  $\text{Fe}_3\text{O}_4$ ,  $\text{MgO}$ ,  $\text{SiO}_2$ , and  $\text{ZnO}$  nanoparticles, have been used as solid adsorbents due to their easy synthesis from an extensive supply of naturally occurring minerals, strong adsorption capacity, surface reactivity, and destructive adsorbents when compared to their

commercial analogs [28]. In comparison to other metals,  $\text{ZnO}$  has various chemical and physical properties such as high electron transfer, wide band range, dielectric properties, low cost, and environmentally friendly characteristics. The remarkable performance and structure of  $\text{ZnO}$ -NFs have recently piqued curiosity due to their structure. Because of its flower-like form, it is preferred for its physicochemical characteristics [29, 30].

The present work aims to prepare a new bioactivated carbon from date palm fronds (AC) using zinc chloride as activating agent, nano zinc oxide (NZ), and nano zinc oxide/activated carbon composite (NZAC). Various techniques and methods were utilized for the characterization of all synthesized solid materials such as TGA, SEM, TEM, FTIR,  $\text{N}_2$  adsorption/desorption studies, and  $\text{pH}_{\text{PZC}}$ . Different application conditions such as the effect of adsorbent dosage, solution pH, time, MB initial concentration, and temperature were studied. Desorption of methylene blue from the surface of the AC sample was studied using different eluents.

## 2 Materials and methods

### 2.1 Materials

Date palm fronds were collected from Al-Wishayl agricultural lands, Al-Rustaq, Sultanate of Oman. The date palm fronds were washed for the removal of any impurities with hot distilled water, dried at 105 °C, and then ground into fine particles. Methylene blue (>98%), polyethylene glycol (40% w/w), zinc chloride (>98%), zinc acetate (>99.99%), and ammonium hydroxide (28%) were obtained from Sigma-Aldrich Co., St. Louis, MO, USA. Hydrochloric acid (37%), ethanol (99%), propanol (>99.8%), sodium chloride (99.95%), and sodium hydroxide ( $\geq 98\%$ ) were purchased from Oxford Lab Fine-Chem Llp Co., India. All chemicals were utilized without any purification.

### 2.2 Synthesis of solid adsorbents

#### 2.2.1 Preparation of zinc chloride-activated carbon (AC)

To prepare activated carbon, the powder of dried date palm fronds (DPF) was soaked in zinc chloride in the ratio (1:3, DPF: $\text{ZnCl}_2$ ) by using an appropriate amount of water for 48 h followed by drying for 24 h at 110 °C. The dry product was pyrolyzed in a stainless steel reactor (70×4 cm) with nitrogen gas flowing at 550 °C and a heating rate of 15 °C/min for 4 h, and then cooled to room temperature. The resulting activated carbon mass was then washed with deionized water until free filtrate from zinc ions. The purified zinc chloride-activated carbons were dried at 110 °C for 24 h [31].

### 2.2.2 Synthesis of zinc oxide nanoparticles (NZ)

To synthesize zinc oxide nanoparticles, 0.5 g of zinc acetate was dissolved in 150 mL distilled water and stirred for 2 h in the presence of polyethylene glycol as capping agent. A few drops of ammonium hydroxide (0.01 mol/L) were added dropwise. The precipitate was then collected using centrifugation process, washed with distilled water, dried at 110 °C, and then calcined for 3 h at 550 °C [32].

### 2.2.3 Preparation of nano zinc oxide/activated carbon composite

Nano zinc oxide/activated carbon composite was synthesized based on the technique described by Esraa et al. with some changes [33]. It is prepared by adding 0.5 g of zinc acetate into 150 mL distilled water in a 250-mL beaker in the presence of polyethylene glycol as capping agent and stirred for 15 min. Then, 3 g of fine powder activated carbon was well dispersed into the previous solution for 10 min. After complete homogeneity, a few drops of NH<sub>4</sub>OH (0.01 mol/L) were added dropwise. The precipitate was then filtered, washed with distilled water, dried at 110 °C, and then calcined for two hours at 550 °C.

## 2.3 Characterization of the prepared solid samples

Thermogravimetric analysis for DPF, AC, NZ, and NZAC adsorbents was determined by a thermal analyzer (NETZCH STA 409, Germany) apparatus at a heating rate of 15 °C/min up to 800 °C and N<sub>2</sub> flow rate of 50 mL/min.

Nitrogen adsorption/desorption studies for AC, NZ, and NZAC were employed at −196 °C by a NOVA 3200e gas sorption analyzer (Quantachrome Corporation, USA) to determine average pore radius ( $\bar{r}_V$ ), total pore volume ( $V_T$ ), and specific surface area ( $S_{BET}$ ). For the sample preparation, about 0.02 g of the sample was placed into a dry and clean sample holder, and then the temperature was raised to 150 °C and degassed for a definite time between 20 and 24 h under reduced pressure of 10<sup>−5</sup> Torr. celli.

The point of zero charges (pH<sub>PZC</sub>) of AC, NZ, and NZAC was studied by adding 0.1 mol/L of NaCl (25 mL) in several closed bottles. The values of initial pH (pH<sub>i</sub>) were adjusted from 2 to 12 by using 0.05 mol/L NaOH and/or HCl. Solid samples (0.025 g) were mixed with bottles and agitated for 24 h. The values of final pH (pH<sub>f</sub>) were determined using a pH meter. The pH<sub>PZC</sub> is defined as the point at which pH<sub>f</sub> − pH<sub>i</sub> = 0 [34].

Fourier transform infrared spectroscopy (Mattson 5000 FTIR spectrometer, San Mateo, CA, USA) was performed for the solid adsorbents in the range 400 to 3800 cm<sup>−1</sup> using a Mattson 5000 FTIR spectrometer to investigate the surface chemical functional groups.

Scanning electron microscope (SEM) was investigated for AC, NZ, and NZAC using a JEOL JSM-6510LV model. The samples were prepared by direct deposition of sample on an aluminum holder and then followed by sputter coating with a thin gold layer with an accelerating voltage of 15 kV under a high vacuum to provide a homogeneous surface for the correct analysis and imaging.

Transmission electron microscopy (TEM) was studied for all solid samples by a JEOL-JEM-2100 model operating at 200 kV. Approximately, 10 mg of the sample was dispersed in ethanol for 45 min using sonication and then transferred to a copper grid. The sample was then taken to dry in the vacuum desiccator for 24 h before commencing the measurements.

## 2.4 Adsorption studies of methylene blue dye

Methylene blue adsorption from aqueous solution by AC, NZ, and NZAC was investigated by shaking MB solution (50 mL) having a definite concentration with 0.05 g of the solid adsorbent for 24 h, pH 7, and at 20 °C. Then, Whatman filter paper (Grade 40) was utilized for the filtration of the supernatant, the first 10 mL from the filtrate was removed, and the concentration of unadsorbed MB concentration was determined using a UV–Vis spectrophotometer at  $\lambda_{max}$  of 663 nm. The equilibrium adsorption capacity ( $q_e$ , mg/g) and removal percentage ( $R\%$ ) were calculated using Eqs. 1 and 2, respectively:

$$q_e = \frac{(C_i - C_e)}{W} \times V \quad (1)$$

$$R\% = \frac{C_i - C_e}{C_i} \times 100 \quad (2)$$

where  $C_i$  and  $C_e$  (mg/L) are the initial and final MB dye concentrations in the solution, respectively.  $V$  (L) is the volume of the solution and  $W$  (g) is the mass of the adsorbent. Various adsorption conditions were used for studying MB such as the effect of pH (2–12), initial concentration of MB (35–540 mg/L), shaking time (0.4–24.0 h), adsorbent dosage (0.25–1.62 g/L), and at temperature (20, 30, and 40 °C).

## 2.5 Adsorption kinetic models

The rate and mechanism of methylene blue adsorption onto the synthesized solid adsorbents were investigated by the linear equations of the pseudo-first-order (PFO, Eq. 4), pseudo-second-order (PSO, Eq. 5), and Elovich (Eq. 6) kinetic models [35]:

$$q_t = \frac{(C_i - C_t)V}{W} \quad (3)$$

$$\ln(q_e - q_t) = \ln q_e - k_1 t \quad (4)$$

$$\frac{t}{q_t} = \frac{1}{k_2 q_e^2} + \frac{1}{q_e} t \quad (5)$$

$$q_t = \frac{\ln \alpha \beta}{\beta} + \frac{1}{\beta} \ln t \quad (6)$$

where  $q_e$  and  $q_t$  (mg/g) are the amounts of methylene blue adsorbed at equilibrium and at time  $t$  (h), respectively.  $k_1$  ( $\text{h}^{-1}$ ),  $C_t$  (mg/L), and  $k_2$  (g/mg.h) are the rate constant of PFO, the residual MB concentration at time  $t$ , and the rate constant of PSO model, respectively.  $\beta$  (g/mg) and  $\alpha$  (mg/g.h) represent the extent of surface coverage and the initial rate of MB adsorption, respectively.

## 2.6 Adsorption isotherm models

Langmuir isotherm model (Eq. 7) shows that the adsorption of adsorbates onto a homogenous surface is monolayer and is explained as follows [36]:

$$\frac{C_e}{q_e} = \frac{1}{b q_m} + \frac{C_e}{q_m} \quad (7)$$

where  $q_e$  and  $q_m$  (mg/g) are equilibrium and maximum adsorption capacity, respectively.  $b$  (L/mg) and  $C_e$  (mg/L) are Langmuir adsorption constant and equilibrium concentration, respectively. Dimensionless separation factor ( $R_L$ ) was calculated to determine the nature of MB adsorption, if it is favorable ( $0 < R_L < 1$ ), unfavorable ( $R_L > 1$ ), and irreversible ( $R_L = 0$ ) as shown in the following equation:

$$R_L = \frac{1}{1 + b C_i} \quad (8)$$

Freundlich isotherm model (Eq. 9) discusses multilayer and monolayer adsorption onto heterogeneous surfaces and is expressed using the following equation:

$$\ln q_e = \ln K_F + \frac{1}{n} \ln C_e \quad (9)$$

where  $K_F$  and  $n$  are Freundlich coefficients expressing the adsorption capacity and adsorption intensity, respectively.

Temkin isotherm model (Eq. 10) explains the effect of indirect interactions between adsorbate and adsorbent as follows:

$$q_e = A \ln K_T + A \ln C_e \quad (10)$$

$$A = \frac{RT}{b_T} \quad (11)$$

Herein,  $R$ ,  $T$ , and  $A$  are the gas adsorption constant (8.314 J/mol.K), the absolute temperature in Kelvin, and the adsorption heat constant, respectively.  $b_T$  (J/mol) and  $K_T$  (L/g) are Temkin constants.

## 2.7 Thermodynamic studies

Thermodynamic adsorption parameters such as the change in entropy ( $\Delta S^\circ$ , kJ/mol. K), free energy ( $\Delta G^\circ$ , kJ/mol), and enthalpy ( $\Delta H^\circ$ , kJ/mol) were considered.  $\Delta S^\circ$  and  $\Delta H^\circ$  values were calculated from the intercept and the slope of Van't Hof plot (Eq. 13) and were discussed by the following equations:

$$K_d = \frac{C_s}{C_e} \quad (12)$$

$$\ln K_d = \frac{\Delta S^\circ}{R} - \frac{\Delta H^\circ}{RT} \quad (13)$$

$$\Delta G^\circ = \Delta H^\circ - T \Delta S^\circ \quad (14)$$

where  $C_e$  and  $C_s$  (mg/L) are concentration at the equilibrium of MB in the solution and MB concentration on the adsorbent, respectively.  $T$  (K),  $R$ , and  $K_d$  are the absolute temperature, gas constant, and adsorption distribution constant, respectively.

## 2.8 Desorption of methylene blue dye

The desorption experiment was conducted on AC to discuss the possibility of reusing the sample in the adsorption process. MB adsorbed onto the surface was desorbed by shaking 0.1 g of MB pre-loaded AC with 50 mL of distilled water, ethanol, propanol, or 0.01 mol/L HCl for 3 h. The previous mixture was filtered, and the desorbed MB was measured in the filtrate [37]. The desorbed quantity was calculated using the following equation:

$$\text{Desorption\%} = \frac{q_i - q_f}{q_i} \times 100 \quad (15)$$

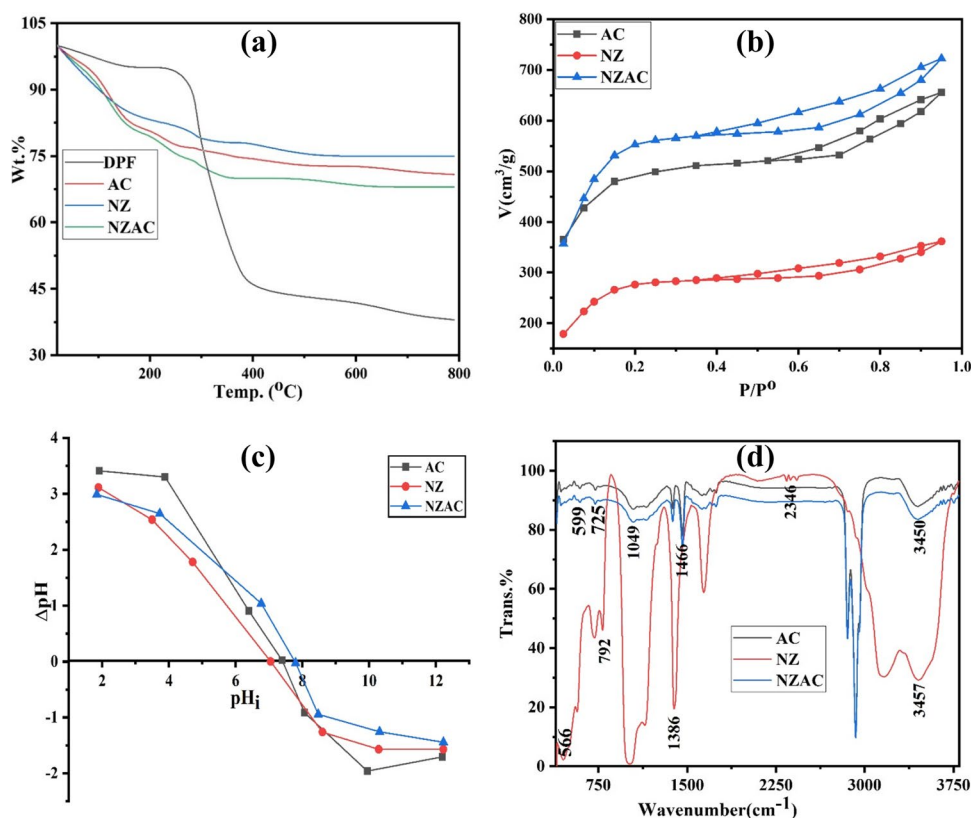
where  $q_i$  and  $q_f$  are the mass (mg) of MB on AC before and after desorption, respectively.

## 3 Results and discussion

### 3.1 Characterization of the synthesized solid adsorbents

The thermogravimetric analysis (TGA) was examined at a temperature of up to 800 °C to determine the thermal

**Fig. 1** TGA (a), nitrogen adsorption/desorption isotherms (b),  $pH_{PZC}$  (c), and FTIR (d), respectively



stability of manufactured solid samples. Figure 1a represents TGA for DPF, AC, NZ, and NZAC samples. Decomposition of DPF occurs in three stages; the initial stage occurs at a temperature up to 151.8 °C with weight loss of about 4.8%. That is a result of the release of water and some light volatile components. Ordinarily, beyond 210 °C, the lignocellulosic structure begins to decompose. The second stage is between 250.3 and 398.5 °C with weight loss of 6.1–54.5%. The rapid conversion of hemicelluloses and cellulose to gases and tars during this stage is thought to be the cause of the significant weight loss that happened. On the other hand, lignin slowly transformed into fumes and tar, and this stage also signifies the start of the generation of carbon. Finally, the third stage happens more than 600 °C with 59.6% weight loss and the weight loss in this stage is gradually decreased and complete degradation of lignin occurs. TGA of DPF shows that its carbonization happens at about 410 °C [19, 38]. NZ degrades through two steps; the first stage is located at a temperature less than 184.50 °C with about 16.96% weight loss because of the evaporation of the surface-adsorbed water, while the second step occurs at higher temperatures (up to 450.72 °C) with weight loss of about 23.84% which is due to the removal of residual oxygen functionalities. The stability of NZ was observed above 450.72 °C indicating the phase transition events and crystallization of NZ nanoparticles [39–41]. As shown in Fig. 1a, three distinct mass loss phases are observed for the AC and

NZAC samples. The first stage is up to 133.10 °C with 13.74 and 15.18% weight loss, respectively, which is attributed to surface-adsorbed water evaporation. The second stage is between 160.32 and 270.75 °C with extra weight loss of about 5.6% and of 7.22% for AC and NZAC, respectively, which is owing to organic compounds decomposition and material structure destruction. The third step, which occurs up to 400 °C with a weight loss of about 25.65 and 29.98% for AC and NZAC, respectively, could be due to the degradation of the material's structure and oxidation of carbon [39, 42]. Whereas NZAC exhibited weight loss of approximately 30.17% up to 459.79 °C, it is evident that impregnation caused a reduction in carbon content and as a result of a reduction in weight loss. It is observed that the stability of NZ > AC > NZAC > DPF is related to the modification of AC by NZ that affect the structure of AC during the formation of composite (NZAC) and leads to the decrease of samples stability, in addition to the least stability of DPF as organic material [19].

The textural parameters such as porosity, surface area, micropore volume, mesopore volume, and total pore volume are crucial for solid adsorbents. Figure 1b represents nitrogen adsorption isotherms and Table 1 shows the textural characteristics of AC, NZ, and NZAC solid adsorbents. According to IUPAC classification, NZ, AC, and NZAC samples showed type (II) adsorption isotherms which confirm the presence of micropores for all samples where

**Table 1** Parameters of  $\text{pH}_{\text{PZC}}$  and nitrogen adsorption for AC, NZ, and NZAC solid samples

Adsorbents	$\text{pH}_{\text{PZC}}$	$S_{\text{BET}}$ ( $\text{m}^2/\text{g}$ )	$V_{\text{T}}$ ( $\text{cm}^3/\text{g}$ )	$V_{\text{micro}}$ ( $\text{cm}^3/\text{g}$ )	$V_{\text{meso}}$ ( $\text{cm}^3/\text{g}$ )	$\bar{r}$ (nm)
AC	7.39	1854.24	0.858	0.749	0.109	0.925
NZ	7.04	1033.42	0.473	0.375	0.098	0.915
NZAC	7.80	2085.47	0.960	0.694	0.266	0.921

average pore radius for AC, NZ, and NZAC were calculated to be 0.925, 0.915, and 0.921 nm, respectively [43, 44]. After examining the information in Table 1, we noted that the specific surface area ( $\text{m}^2/\text{g}$ ) of NZAC (2085.47) > AC (1854.24) > NZ (1033.42) and total pore volume ( $\text{cm}^3/\text{g}$ ) of NZAC (0.960) > AC (0.858) > NZ (0.473), increasing specific surface area with increasing total pore volume and indicating the highly porous nature of the resulted nanocomposite (NZAC). The ratio of micropore to mesopore volumes was found to be 6.9, 3.8, and 2.6, respectively, in the cases of AC, NZ, and NZAC when we estimated the micropore and mesopore volumes using the Gomez-Serrano method [45]. This demonstrates that more microporosity is created when AC was activated with zinc chloride. The unique increase in specific surface area from 1033.42 to 2085.47  $\text{m}^2/\text{g}$ , indicating the increase of active sites and pores on the NZAC surface and proving its higher adsorption capacity.

The calculated values of point of zero charges ( $\text{pH}_{\text{PZC}}$ ) for AC, NZ, and NZAC samples are 7.39, 7.04, and 7.80, respectively, as displayed in Fig. 1c and listed data in Table 1.

FTIR spectra of AC, NZ, and NZAC solid adsorbents are illustrated in Fig. 1d to analyze their surface chemical functional groups. Bands at 1386, 2346, and 3457  $\text{cm}^{-1}$  on NZ are connected to the stretching vibration of the OH group, the (O=C=O) functionality of absorbed  $\text{CO}_2$ , and the OH bending of water obtained by moisture absorption from the air, respectively. The peaks located at 566 and 792  $\text{cm}^{-1}$  showed stretching vibration of ZnO, indicating NZ's successful synthesis [46], whereas FTIR for AC and NZAC depicts the same broadband at 3450  $\text{cm}^{-1}$  which confirmed the OH stretching vibration of surface-adsorbed water, while the observed bands located at 1049 and 1466  $\text{cm}^{-1}$  indicated C=O stretching vibration. Peaks at 599 and 725  $\text{cm}^{-1}$  in FTIR of composite (NZAC) are attributed to ZnO stretching vibration. The acetate groups C=O and C-O stretching vibrations are responsible for the maxima at around 1700 and 1070  $\text{cm}^{-1}$ , respectively [33]. The previous result confirms the formation of composite. The data of FTIR illustrated the excellent preparation of nano samples, and NZAC composite contains both zinc oxide and activated carbon [47].

The surface morphology, shape, and size of AC, NZ, and NZAC samples were evaluated by SEM analysis as shown in Fig. 2. The SEM image of the AC sample indicated that

the surface of AC is highly porous, uneven, and rough with deep holes and grooves [48]. The NZ image appears as a circle and hexagonal shape with aggregated and irregular morphology [49], while NZAC image demonstrated the nanocomposite's agglomerated shape, and the observable aggregation in the created nanocomposite looks toward the effective blending of AC and NZ nanoparticles. Although AC's pores were largely closed by its immobilization in the NZ matrix, the composite nevertheless exhibits a porous nature and has a substantial surface area. This is possible because the exterior surfacing was the most accessible, preventing NZ from entering the interior micropores of the AC. Smaller-sized pores, however, were still open [47, 50].

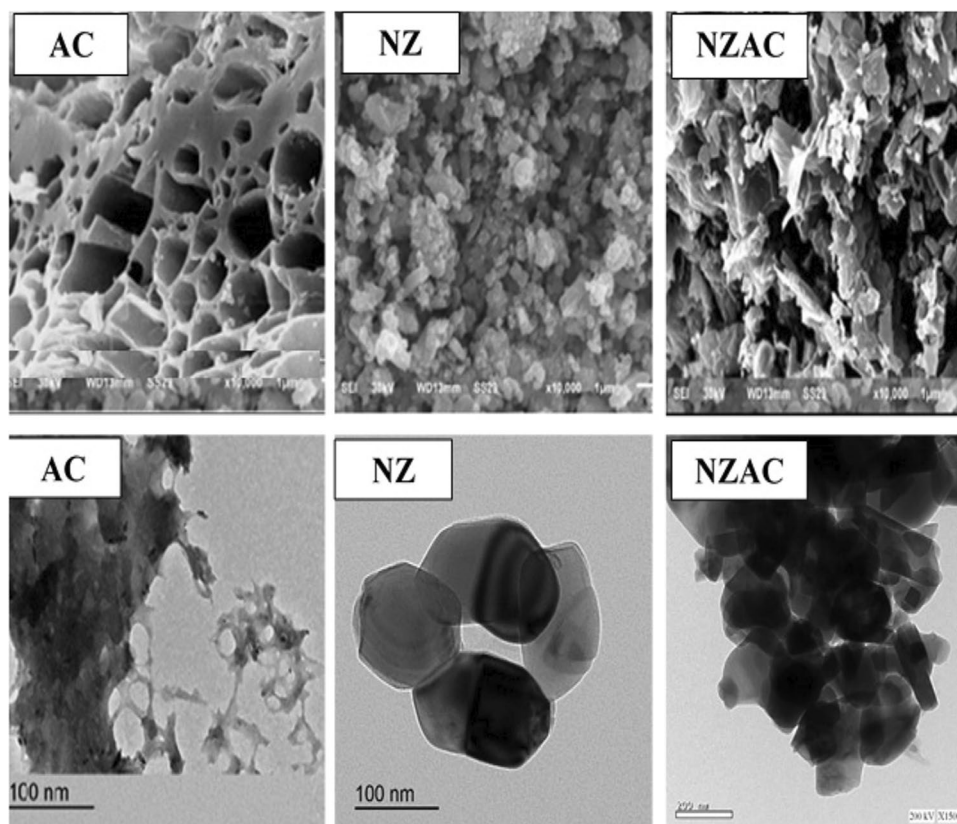
TEM micrographs are displayed in Fig. 2 for AC, NZ, and NZAC. TEM image for AC indicated a disordered and porous hierarchical structure, containing both microporous and mesoporous with a particle size of 30–100 nm [51]. For the NZ sample, the particles appear as elongated ellipsoidal with a larger diameter in the middle and a particle size of 70–100 nm [52], while in the NZAC image, it is observed both circle and elongated particles, and NZ are equally distributed through an AC blended with a particle size of 50 nm.

## 3.2 Methylene blue adsorption

### 3.2.1 Effect of adsorbent dosage

Figure 3a displays the relation between the adsorbent dosage (g/L) and the removal percentage (Eq. 2) of MB through a 0.25–1.62 g/L range of adsorbent dosage at pH 7 and 30 °C for 24 h. By increasing the adsorbent dosage from 0.25 to 1.62 g/L, the removal percentage for AC, NZ, and NZAC, respectively, increased from 3.9, 3.8, and 10% to 70, 55, 83% by 17.5, 13.8, and 8.3 times, respectively. Where, as the adsorbent dosage increased, the observable sharp enhancement in the MB removal% occurred and is attributed to the existence of more active surface sites for MB adsorption [34, 35]. At higher adsorbent amount ( $\hat{>}$  1.38 g/L), the increment in the active sites had a little influence on the removal percentage because of the establishment of equilibrium at low methylene blue concentration in the medium of adsorption before the saturation. Because NZAC has a larger surface area

**Fig. 2** SEM and TEM images for AC, NZ, and NZAC, respectively



and more chemical functional groups, it has a greater  $R\%$  than AC and NZ. Upon the previous results, the optimum adsorbent dosage of 1 g/L was selected for AC, NZ, and NZAC.

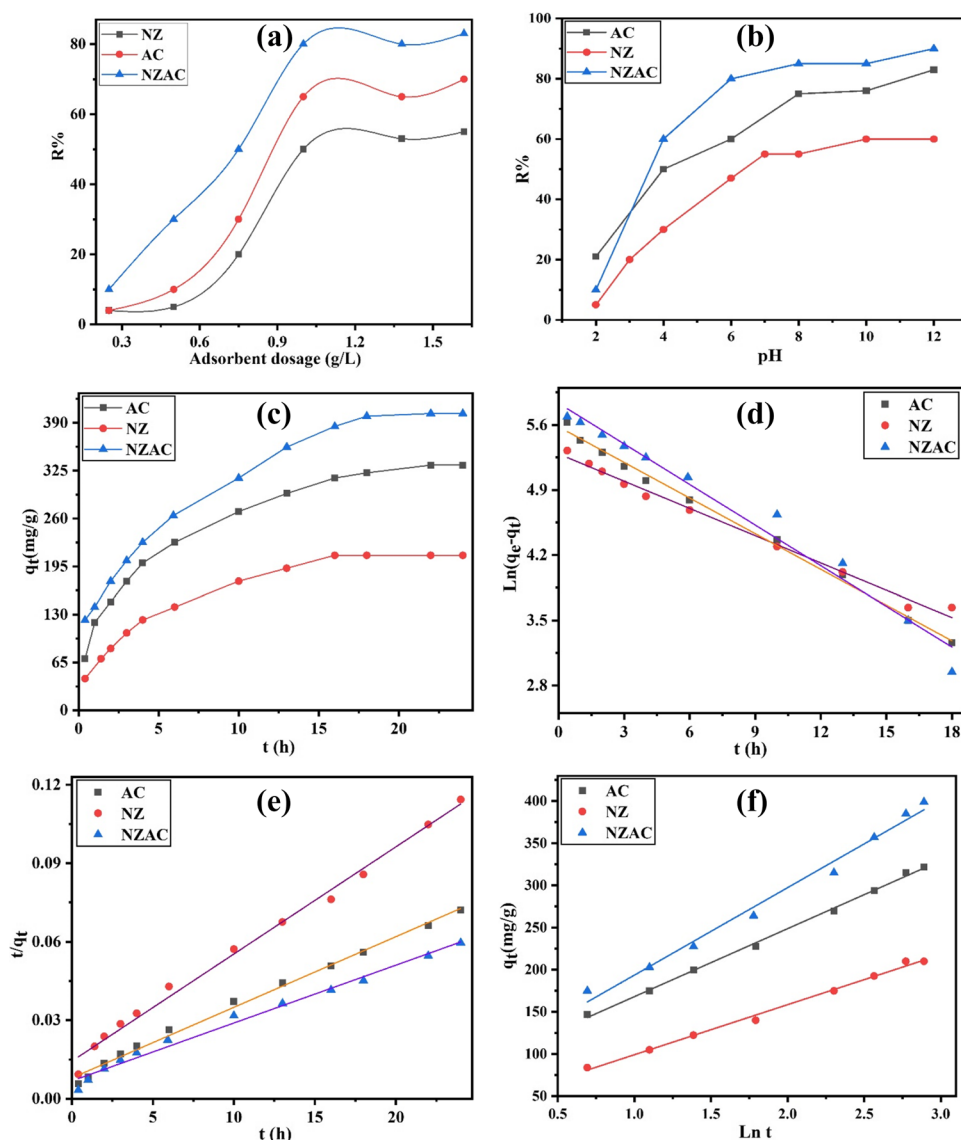
### 3.2.2 Effect of pH

It is well known that the adsorption degree of ionic dyes onto the surface of adsorbent is primarily affected by the surface's charge on the solid adsorbent that is affected by the pH of solution. Figure 3b portrays the pH effect on the MB removal percentage by AC, NZ, and NZAC, where  $R\%$  increased from 21, 5, 10% to 83, 60, 90% by 4, 12, 9 times for AC, NZ, and NZAC, respectively through pH range from 2 to 12. The increment in MB adsorption with increasing pH values is owing to the increment in electrostatic attraction between the negatively charged adsorbent surface and positively charged MB and the reduction in the protonation of surface of adsorbent with increasing pH values more than  $\text{pH}_{\text{PZC}}$  (7.39, 7.04, and 7.80 for AC, NZ, and NZAC, respectively). The increase of removal percent of MB is slowdown at pH values  $> 8$ . Equilibrium pH occurred at  $\text{pH} > \text{pH}_{\text{PZC}}$ . Lower removal of methylene blue in acidic solution may be due to the protons competition with MB dye for the available active adsorption sites [53].

### 3.2.3 Effect of shaking time and kinetic studies

An important aspect of determining the equilibrium time and adsorption kinetics is the impact of shaking contact time on the removal of organic hazardous bulky contaminants by adsorption. The plot between the shaking time and the adsorbed mass of methylene blue ( $q_t$ , mg/g) at 30 °C in the range of 0.4 to 24.0 h is depicted in Fig. 3c. It was observed that the adsorption rate is extremely fast in the first 10 h because of the availability of active surface sites onto the prepared samples [54]. Methylene blue adsorption enhanced until the equilibrium time was occurred after 16 h for AC and NZAC while after 13 h for NZ and that is related to the lower surface area of NZ, where the adsorption capacity increased by 4.5, 4.5, and 3.1 folds for AC, NZ, and NZAC, respectively through the equilibrium time. After the equilibrium time, the adsorption rate decreased owing to the saturation of surface of adsorbent and the completeness of monolayer of methylene blue dye onto the surface. Figure 3d–f shows PFO (Eq. 4), PSO (Eq. 5), and Elovich (Eq. 6) kinetic models and kinetic parameters for methylene blue adsorption are listed in Table 2. Whereby the results in Table 2, (i) methylene blue adsorption onto the solid samples was not fitted by pseudo-first-order model according to the high variation between the adsorption capacities ( $q_m$ ) of Langmuir and calculated values

**Fig. 3** Effect of adsorbent dosage (a), pH (b), shaking time (c), pseudo-first-order (d), pseudo-second-order (e), and Elovich (f) plots for the MB adsorption onto AC, NZ, and NZAC



( $q_{exp}$ ) (30.3, 37.3, and 27.2% for AC, NZ, and NZAC, respectively); however, the correlation coefficients ( $R^2$ ) (0.9744–0.9948) are high. (ii) PSO kinetic model applied well the MB adsorption onto all the prepared solid adsorbents based on the small variation between  $q_{exp}$  and  $q_m$  values (0.2, 7.6, and 4.0% for AC, NZ, and NZAC, respectively) besides the high  $R^2$  (0.9867–0.9939). (iii) The PSO rate constants ( $k_2$ ) follow the sequence  $NZ > AC > NZAC$  ( $1.17 \times 10^{-3}$ ,  $9.18 \times 10^{-4}$ , and  $7.16 \times 10^{-4}$  g/mg.h, respectively), indicating the higher attraction binding between the surface functional groups onto NZ and the cationic MB dye. (iv) Correlation coefficients ( $> 0.9852$ ) of Elovich kinetic model affirmed its best fitting for MB adsorption. The initial rate ( $\alpha$ ) values follow the trend  $NZAC > AC > NZ$ , revealing the increment in the adsorption capacity, and  $\beta$  trend ( $NZ > AC > NZAC$ ) concurred with the trend of PSO rate constant ( $k_2$ ) values confirmed the completeness

of surface coverage onto NZ firstly due to its lower surface area and chemical functional groups.

### 3.2.4 Effect of temperature and adsorption isotherms

Adsorption isotherms play an essential role to investigate the maximum adsorption capacities. Adsorption isotherms link the adsorbed MB amounts to the remaining MB concentration in an aqueous solution and determine the adsorbent capacity and the adsorbate affinity to the solid adsorbent surface. Effect of various temperatures (20, 30, and 40 °C) was studied for methylene blue adsorption onto the solid adsorbents (AC, NZ, and NZAC) at pH 7, 35–540 mg/L of initial MB concentration, adsorbent dosage of 1 g/L, and for 24 h of contact time as displayed in Fig. 4a–c. Figure 4a–c illustrates that at the beginning of the initial increase in MB concentration, there is highly obvious increment in



**Table 2** Kinetic parameters of pseudo-first-order, pseudo-second-order, Elovich, and thermodynamic parameters for the MB adsorption onto the surface of AC, NZ, and NZAC at 30 °C

Solid samples	Parameters	AC	NZ	NZAC	
PFO	$q_m$ (mg/g)	380.23	315.46	434.78	
	$q_{exp}$ (mg/g)	265.07	197.90	316.67	
	$k_1$ (h <sup>-1</sup> )	0.1278	0.0978	0.1456	
	$R^2$	0.9948	0.9900	0.9744	
PSO	$q_{exp}$ (mg/g)	379.36	291.26	452.49	
	$k_2$ (g/mg.h)	$9.18 \times 10^{-4}$	$1.17 \times 10^{-3}$	$7.16 \times 10^{-4}$	
	$R^2$	0.9939	0.9921	0.9867	
Elovich	$\alpha$ (mg/g.h)	238.45	116.18	246.66	
	$\beta$ (g/mg)	0.0124	0.0168	0.0096	
	$R^2$	0.9975	0.9942	0.9852	
Thermodynamic parameters	$R^2$	0.9763	0.9856	0.9676	
	$\Delta H^\circ$ (kJ/mol)	5.128	7.095	3.561	
	$\Delta S^\circ$ (kJ/mol. K)	0.0278	0.0316	0.0243	
	$\Delta G^\circ$ (kJ/mol)	20 °C	- 3.0174	- 2.1638	- 3.5589
		30 °C	- 3.2954	- 2.4798	- 3.8019
40 °C		- 3.5734	- 2.7958	- 4.0449	

the adsorption capacities ( $q_e$ , mg/g) and started to remain stable at a higher initial MB concentrations because of the completeness of surface coverage. Several adsorption isotherm models (Langmuir, Freundlich, and Temkin models, Eqs. 7, 9, and 10, respectively) were studied to investigate the adsorption isotherm data as analyzed in Table 3.

Langmuir isotherm model describes the adsorbent atoms' monolayer retention on a uniform surface. Based on the higher regression coefficients ( $R^2$ , 0.9814–0.9974), Langmuir adsorption model matched well with the MB adsorption onto the prepared samples as shown in Fig. 4d–f. Adsorption capacities of NZAC > AC > NZ at all the temperatures are related to the modification of activated carbon with nano zinc oxide and increase of several chemical functional groups onto NZAC surface, besides the higher specific surface area of NZAC. The improvement of adsorption capacity with increasing temperature from 20 to 40 °C testified the endothermic process of MB adsorption onto AC, NZ, and NZAC. Langmuir binding values ( $b$ , L/mg) were promoted with temperature and follow sequence NZAC > AC > NZ, indicating the higher attraction force between NZAC and MB dye, especially at higher temperature [55]. The  $R_L$  values (0.014–0.119) calculated from Eq. 8 reveal the highly favorable MB adsorption onto the prepared adsorbents.

Freundlich isotherm plots of AC, NZ, and NZAC for the MB adsorption at different temperature are depicted in Fig. 5a–c. Adsorption of methylene blue follows well Freundlich model according to the higher  $R^2$  values (> 0.9689) upon the data in Table 3. The  $K_F$  values increased with raising temperature for all the adsorbents as with adsorption capacity of Langmuir. Also, the values of  $1/n$  (<1) indicated the physical methylene blue adsorption onto NZ, AC, and NZAC. The decrease in adsorption intensity ( $1/n$ ) with

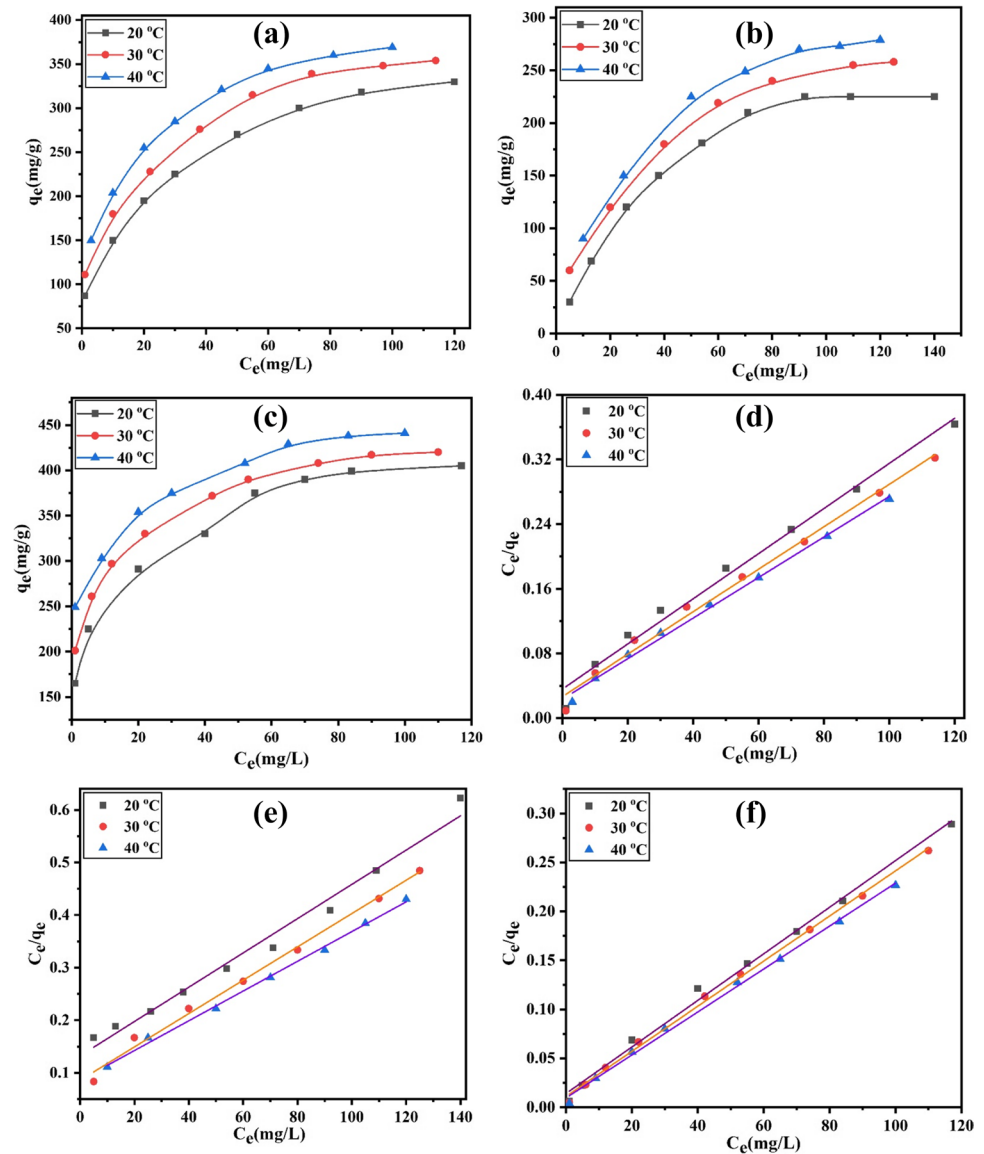
temperature achieved the enhancement of surface heterogeneity. Furthermore,  $1/n$  values ( $0.1 < 1/n < 1.0$ ) ranged from 0.1319 to 0.6996 verified the MB adsorption favorability [56].

Figure 5d–f displays the plots of Temkin isotherm model for MB adsorption onto AC, NZ, and NZAC at 20, 30, and 40 °C and the findings are listed in Table 3. The best description of Temkin model for MB adsorption demonstrated from the higher  $R^2$  values (0.9238–0.9871). The increment of Temkin constant ( $K_T$ ) values with the increase in temperature assessed the endothermic process of MB adsorption [57]. The Temkin constant ( $b_T$ ) values (32.45–58.37 J/mol) confirmed the physical adsorption ( $b_T < 8000$  J/mol) of MB onto the solid adsorbents [58].

### 3.2.5 Thermodynamic study

Thermodynamic parameters ( $\Delta H^\circ$ ,  $\Delta S^\circ$ , and  $\Delta G^\circ$ ) were calculated in Eqs. 12–14, and their outcomes are found in Table 2. Upon inspection of the findings in Table 2, (i) the increase in methylene blue randomness close to the solid surface throughout the adsorption process is shown by the positive entropy change values (0.0243–0.0316 kJ/mol. K). (ii) The positive  $\Delta H^\circ$  values (3.561–7.095 kJ/mol) prove the endothermic process of MB adsorption onto the studied solid adsorbents. Moreover, the enthalpy change values (< 40 kJ/mol) assert the physisorption of MB [59]. (iii) The adsorption process' spontaneity and viability at the examined temperatures onto all of the samples are confirmed by the negative free energy change values. The promotion of negativity of  $\Delta G^\circ$  values with the temperature reflects the improvement of adsorption at higher temperature. (iv) The estimated  $\Delta G^\circ$  values (- 2.1638 to - 4.0449) exhibit

**Fig. 4** Adsorption isotherms of MB (a, b, and c) and linear Langmuir plots (d, e, and f) for AC, NZ, NZAC, respectively at 20, 30, and 40 °C



**Table 3** Parameters of Langmuir, Freundlich, and Temkin for MB adsorption onto AC, NZ, and NZAC at 20, 30, and 40 °C

Samples	AC			NZ			NZAC		
	20 °C	30 °C	40 °C	20 °C	30 °C	40 °C	20 °C	30 °C	40 °C
Langmuir parameters									
$q_m$ (mg/g)	358.42	380.23	398.41	306.75	315.46	353.36	420.17	434.78	456.62
$b$ (L/mg)	0.078	0.098	0.107	0.025	0.032	0.036	0.170	0.209	0.230
$R_L$	0.041	0.033	0.030	0.119	0.083	0.092	0.019	0.016	0.014
$R^2$	0.9852	0.9896	0.9952	0.9814	0.9922	0.9967	0.9939	0.9974	0.9969
Freundlich parameters									
$1/n$	0.2924	0.2694	0.2580	0.6996	0.4689	0.4651	0.1969	0.1644	0.1319
$K_F$	83.34	106.86	112.81	10.89	29.57	32.81	164.22	198.79	240.92
$R^2$	0.9892	0.9868	0.9920	0.9790	0.9802	0.9689	0.9924	0.9955	0.9764
Temkin parameters									
$K_T$ (L/g)	1.90	3.00	3.31	0.25	0.34	0.35	16.41	40.49	178.52
$b_T$ (J/mol)	45.35	45.85	39.26	34.87	38.35	32.45	45.44	50.36	58.37
$R^2$	0.9238	0.9348	0.9854	0.9825	0.9756	0.9871	0.9697	0.9801	0.9506

**Fig. 5** Linear Freundlich (a, b, and c) and Temkin (d, e, and f) plots for the MB adsorption onto AC, NZ, and NZAC, respectively at 20, 30, and 40 °C

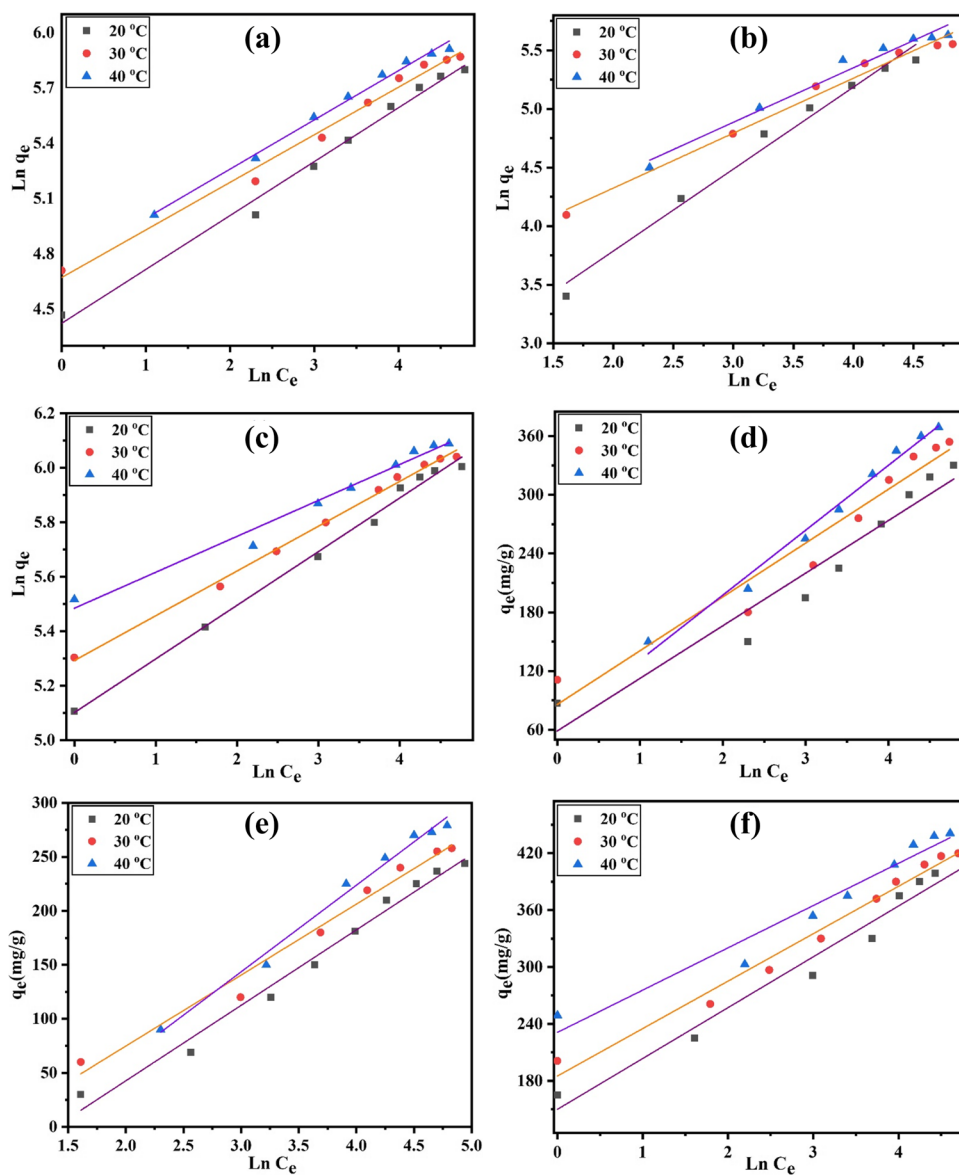
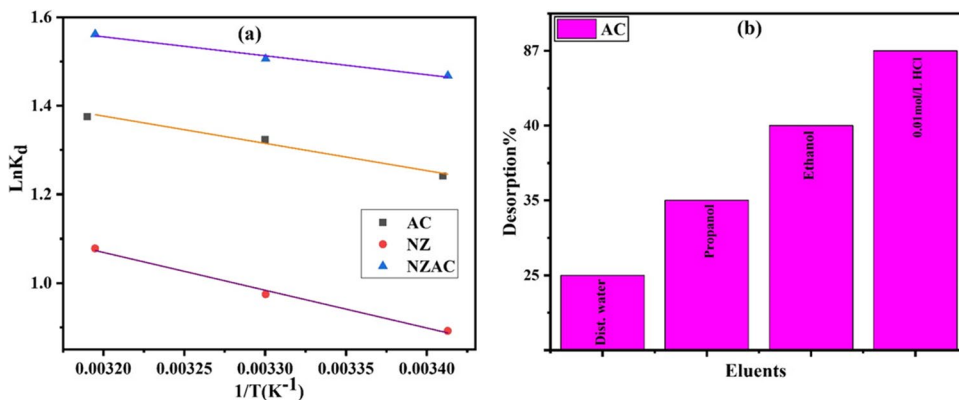


**Fig. 6** Van't Hoff plot (a) and MB desorption from AC using different eluents (b)



the physisorption process of MB onto the solid samples, whereby  $\Delta G^\circ$  values range of physisorption and chemisorption (0 to  $-20$  and  $-400$  to  $-80$  kJ/mol, respectively) [60]. (v) Van't Hoff plot (Fig. 6a) describes well the MB adsorption upon the higher  $R^2$  values ( $> 0.9676$ ). It can be concluded that  $\Delta G^\circ$  values of NZAC  $>$  AC  $>$  NZ verify the best spontaneity and feasibility of MB adsorption onto NZAC surface.  $\Delta H^\circ$  and  $\Delta S^\circ$  values of NZ  $>$  AC  $>$  NZAC agreed with the trend of  $\beta$  and  $k_2$  values, testify the highly endothermic and random nature of adsorption process onto NZ surface.

### 3.3 Desorption study

Figure 6b portrays the desorption percent, calculated by Eq. 15, of MB from AC surface by utilizing various eluents. It was obvious the desorption% for 0.01 mol/L HCl  $>$  ethanol  $>$  propanol  $>$  distilled water (87, 40, 35, and 25%, respectively). That is related to the higher acidity and polarity of inorganic eluents, whereby HCl  $>$  ethanol  $>$  propanol  $>$  distilled water in acidity and polarity, releasing more protons in solution that compete with cationic MB for the adsorption onto AC surface and increasing the electrostatic repulsion between the MB and AC surface in presence of HCl.

### 3.4 Possible mechanism of MB adsorption on NZAC composite

The composite formed by the interaction of zinc chloride-activated carbon with zinc oxide nanoparticles contains several surface chemical functional groups that can interact with the heteroatoms of MB molecules. A number of interactions coexisted during the challenging process of MB adsorption on NZAC. MB is an electrostatically adsorbable cationic dye that may be applied to negatively charged surfaces [61]. Between the hydrogen from composite and the nitrogen from MB, a hydrogen bonding contact was created. Most adsorption systems typically contain hydrogen bonds, which are referred to as non-electrostatic bonding [62]. Additionally, despite being suitable planer molecules, MB molecules can be readily adsorbed by NZAC due to interactions between their aromatic backbones.

### 3.5 Comparison of NZAC with other solid adsorbents

The maximum adsorption capacity of NZAC as a solid sample for MB adsorption in comparison with that of the other adsorbents is shown in Table 4 [1, 4, 12, 14, 34, 50, 54–56, 60, 63]. Based on its greater surface area, the results in Table 4 show that NZAC is a viable solid adsorbent for the removal of methylene blue from wastewater.

**Table 4** Comparison of the maximum adsorption capacity of NZAC with other adsorbents

Adsorbents	$q_m$ (mg/g)	References
ACC film (Activated carbon/cellulose biocomposite film)	103.66	[1]
CNT (Carbon nanotube)	181.81	[4]
Zeolite granules in a fluidized bed	108.04	[12]
Porous biochar	110.38	[14]
NC (Nanomagnetite/potassium carrageenan)	374.50	[34]
AC-ZnO (Activated carbon coated with ZnO)	32.22	[50]
CP11 (Phosphoric acid activated carbon)	403.20	[54]
OPF MCC (Microcrystalline cellulose)	12.85	[55]
Cellulose microfibrils	54.90	[56]
Gar/ $\kappa$ -carrageenan hydrogel	242.30	[60]
Acid washed RS-ZnCl <sub>2</sub> Carbon-ZnO nanocomposites	258.00	[63]
NZAC (Nano zinc oxide/activated carbon composite)	456.62	[This study]

## 4 Conclusion

The present work depicts that date palm fronds were utilized to prepare a new bioactivated carbon and its composite. NZAC demonstrated high thermal stability up to 200 °C, high surface area (2085.47 m<sup>2</sup>/g), pore radius of 0.921 nm, micropore volumes of 0.694 cm<sup>3</sup>/g pH<sub>PZC</sub> of 7.80, several chemical functional groups including  $-OH$ ,  $C=O$ , and ZnO stretching vibration modes, and effective binding between AC and NZ nanoparticles. NZAC showed the higher Langmuir adsorption capacities for methylene blue dye and enhanced with temperature (420.17, 434.78, and 456.62 mg/g at 20, 30, and 40 °C, respectively). Thermodynamic and kinetic studies testified the best fitting for NZAC of Van't Hoff, PSO, and Elovich models ( $R^2 = 0.9676, 0.9867, \text{ and } 0.9852$ , respectively) with endothermic nature, physisorption, and spontaneous process. Hydrochloric acid attained the higher desorption percent (87%) compared with the other eluents. The previous consequences reveal the excellent adsorption nature and unique properties of NZAC in the treatment of wastewater.

**Acknowledgements** The authors would like to extend their sincere appreciation to University of Technology and Applied Sciences.

**Author contribution** All authors contributed to the study conception and design. Material preparation and analysis were performed by *Asaad*

F. Hassa and Laila M. Alshandoudi. Data collection was performed by Said R. Alkindi and Tariq Y. Alhatmi.

**Funding** This study was funded by Ministry of Higher Education, Research and Innovation of Sultanate of Oman through the research group project no. BFI/URG/EBR/21/249.

**Data availability** Not applicable.

## Declarations

**Ethical approval** Not applicable.

**Conflict of interest** The authors declare no competing interests.

## References

- Somsesta N, Sricharoenchaikul V, Aht-Ong D (2020) Adsorption removal of methylene blue onto activated carbon/cellulose biocomposite films: equilibrium and kinetic studies. *Mater Chem Phys* 240:122221. <https://doi.org/10.1016/j.matchemphys.2019.122221>
- Son G, Kim D, Lee JS, Kim H, Lee C, Kim S-R, Lee H (2018) Synchronized methylene blue removal using Fenton-like reaction induced by phosphorous oxoanion and submerged plasma irradiation process. *J Environ Manage* 206:77–84. <https://doi.org/10.1016/j.jenvman.2017.10.024>
- Lokhande KD, Pethsangave DA, Kulal DK, Some S (2020) Remediation of toxic dye pollutants by using graphene-based adsorbents. *Mater Sci Inc. Nanomater Polym* 5(27):8062–8073. <https://doi.org/10.1002/slct.202002130>
- Yadav S, Yadav A, Bagotia N, Sharma AK, Kumar S (2022) Novel composites of Pennisetum glaucum with CNT: preparation, characterization and application for the removal of safranin O and methylene blue dyes from single and binary systems. *Biomass Convers Biorefinery*. <https://doi.org/10.1007/s13399-021-02240-z>
- Soares SF, Simões TR, Trindade T, Daniel-da-Silva AL (2017) Highly efficient removal of dye from water using magnetic carrageenan/silica hybrid nano-adsorbents. *Water, Air, Soil Pollut* 228:87. <https://doi.org/10.1007/s11270-017-3281-0>
- Shahrul AM, Syarifah Adilah MY, Radzali R, Malek MF, Isa IS, Rusop M, Damanhuri NS, Abdullah MH (2022) Low-cost coagulation treatment of dye sensitizer for improved time immersion of dye-sensitized solar cells (DSSC). *Microelectron Eng*. 262:111832. <https://doi.org/10.1016/j.mee.2022.111832>
- Zhao J, Liu H, Xue P, Tian S, Sun S, Lv X (2021) Highly-efficient PVDF adsorptive membrane filtration based on chitosan@CNTs-COOH simultaneous removal of anionic and cationic dyes. *Carbohydr. Polym.* 274:118664. <https://doi.org/10.1016/j.carbpol.2021.118664>
- Zhang X, Jiang S, Sun LX, Xing YH, Bai FY (2022) Synthesis and structure of a 3D supramolecular layered Bi-MOF and its application in photocatalytic degradation of dyes. *J Mol Struct* 1270:133895. <https://doi.org/10.1016/j.molstruc.2022.133895>
- Lu C, Yang J, Khan A, Yang J, Li Q, Wang G (2022) A highly efficient technique to simultaneously remove acidic and basic dyes using magnetic ion-exchange microbeads. *J. Environ. Manage.* 304:114173. <https://doi.org/10.1016/j.jenvman.2021.114173>
- Bravo-yumi N, Alvarez MP, Bandala ER (2022) Studying the influence of different parameters on the electrochemical oxidation of tannery dyes using a Ti/IrO<sub>2</sub>-SnO<sub>2</sub>-Sb<sub>2</sub>O<sub>5</sub> anode. *Chem Eng Process - Process Intensif* 109173. <https://doi.org/10.1016/j.cep.2022.109173>
- Shajeelammal J, Mohammed S, Prathish KP, Jeeva A, Asok A, Shukla S (2022) Treatment of real time textile effluent containing azo reactive dyes via ozonation, modified pulsed low frequency ultrasound cavitation, and integrated reactor. *J Hazard Mater Adv* 7:100098. <https://doi.org/10.1016/j.hazadv.2022.100098>
- Lv B, Dong B, Zhang C, Chen Z, Zhao Z, Deng X, Fang C (2022) Effective adsorption of methylene blue from aqueous solution by coal gangue-based zeolite granules in a fluidized bed: fluidization characteristics and continuous adsorption. *Powder Technol* 408. <https://doi.org/10.1016/j.powtec.2022.117764>
- Wan X, Rong Z, Zhu K, Wu Y (2022) Chitosan-based dual network composite hydrogel for efficient adsorption of methylene blue dye. *Int J Biol Macromol* 222:725–735. <https://doi.org/10.1016/j.ijbiomac.2022.09.213>
- Wu T, Yang G, Cao J, Xu Z, Jiang X (2022) Activation and adsorption mechanisms of methylene blue removal by porous biochar adsorbent derived from eggshell membrane. *Chem Eng Res Des* 188:330–341. <https://doi.org/10.1016/j.cherd.2022.08.042>
- Alam S, Ullah B, Khan MS, Ur Rahman N, Khan L, Shah LA, Zekker I, Burlakovs J, Kallistova A, Pimenov N, Yandri E, Setyobudi RH, Jani Y, Zahoor M (2021) Adsorption kinetics and isotherm study of basic red 5 on synthesized silica monolith particles. *Water (Switzerland)* 13:1–13. <https://doi.org/10.3390/w13202803>
- Zambare R, Song X, Bhuvana S, Prince JSA, Nemade P (2017) Ultrafast dye removal using ionic liquid–graphene oxide sponge. *ACS Sustain Chem Eng* 5(7):6026–6035. <https://doi.org/10.1021/acssuschemeng.7b00867>
- Gao Q, Xu J, Bu XH (2019) Recent advances about metal–organic frameworks in the removal of pollutants from wastewater. *Coord Chem Rev* 378:17–31. <https://doi.org/10.1016/j.ccr.2018.03.015>
- Singh AR, Dhumal PS, Bhakare MA, Lokhande KD, Bondarde MP, Some S (2022) In-situ synthesis of metal oxide and polymer decorated activated carbon-based photocatalyst for organic pollutants degradation. *Sep Purif Technol* 286:120380–120388. <https://doi.org/10.1016/j.seppur.2021.120380>
- Ahmad A, Al-Swaidan HM, Alghamdi AH (2015) Production of activated carbon from raw date palm fronds by ZnCl<sub>2</sub> activation. *J Chem Soc Pakistan* 37:1081–1087
- Ozdemir I, Şahin M, Orhan R, Erdem M (2014) Preparation and characterization of activated carbon from grape stalk by zinc chloride activation. *Fuel Process Technol* 125:200–206. <https://doi.org/10.1016/j.fuproc.2014.04.002>
- Ferrera-Lorenzo N, Fuente E, Suárez-Ruiz I, Ruiz B (2014) KOH activated carbon from conventional and microwave heating system of a macroalgae waste from the Agar-Agar industry. *Fuel Process Technol* 121:25–31. <https://doi.org/10.1016/j.fuproc.2013.12.017>
- Gerçel Ö, Özcan A, Özcan AS, Gerçel HF (2007) Preparation of activated carbon from a renewable bio-plant of *Euphorbia rigida* by H<sub>2</sub>SO<sub>4</sub> activation and its adsorption behavior in aqueous solutions. *Appl Surf Sci* 253:4843–4852. <https://doi.org/10.1016/j.apsusc.2006.10.053>
- Alvarez P, Blanco C, Granda M (2007) The adsorption of chromium (VI) from industrial wastewater by acid and base-activated lignocellulosic residues. *J Hazard Mater* 144:400–405. <https://doi.org/10.1016/j.jhazmat.2006.10.052>
- Sivaraj R, Rajendran V, Gunalan GS (2010) Preparation and characterization of activated carbons from parthenium biomass by physical and chemical activation techniques. *E-Journal Chem* 7:1314–1319. <https://doi.org/10.1155/2010/948015>
- Ncibi MC, Ranguin R, Pintor MJ, Jeanne-Rose V, Sillanpää M, Gaspard S (2014) Preparation and characterization of chemically activated carbons derived from Mediterranean *Posidonia oceanica* (L.) fibres. *J Anal Appl Pyrolysis* 109:205–214. <https://doi.org/10.1016/j.jaap.2014.06.010>

26. Haghbin MR, Niknam Shahrak M (2021) Process conditions optimization for the fabrication of highly porous activated carbon from date palm bark wastes for removing pollutants from water. *Powder Technol* 377:890–899. <https://doi.org/10.1016/j.powtec.2020.09.051>
27. Debnath P, Mondal NK (2020) Effective removal of congo red dye from aqueous solution using biosynthesized zinc oxide nanoparticles. *Environ Nanotechnol Monit Manag* 14:100320. <https://doi.org/10.1016/j.enmm.2020.100320>
28. Sanjid Qais D, Nazrul Islam M, Hafiz Dzarfan Othman M, Ekramul Mahmud HNM, Emran Quayum M, Anwarul Islam M, Mohammad Ibrahim Ismail I, Habib A (2021) WITHDRAWN: Synthesis and characterization of nano-zinc oxide: adsorption of acid blue 92 dye, isotherms, thermodynamics and kinetics. *Arab J Chem* 103627. <https://doi.org/10.1016/j.arabjc.2021.103627>
29. Eskikaya O, Ozdemir S, Tollu G, Dizge N, Ramaraj R, Manivanan A, Balakrishnan D (2022) Synthesis of two different zinc oxide nanoflowers and comparison of antioxidant and photocatalytic activity. *Chemosphere* 306:135389. <https://doi.org/10.1016/j.chemosphere.2022.135389>
30. Norouzi A, Nezamzadeh-Ejehieh A, Fazaeli R (2021) A Copper(I) oxide-zinc oxide nano-catalyst hybrid: brief characterization and study of the kinetic of its photodegradation and photomineralization activities toward methylene blue. *Mater Sci Semicond Process* 122:105495. <https://doi.org/10.1016/j.mssp.2020.105495>
31. Youssef A, EL-Didamony H, Sharabasy SEL-, Sobhy M, Hassan A, Buláneke R (2017) Adsorption of 2, 4 dichlorophenoxyacetic acid on different types of activated carbons based date palm pits: kinetic and thermodynamic studies. *Int Res J Pure Appl Chem* 14:1–15. <https://doi.org/10.9734/irjpac/2017/33073>
32. Elsayed MS, Ahmed IA, Bader DMD, Hassan AF (2021) Green synthesis of nano zinc oxide/nanohydroxyapatite composites using date palm pits extract and eggshells: adsorption and photocatalytic degradation of methylene blue. *Nanomater (Basel, Switzerland)* 12. <https://doi.org/10.3390/nano12010049>
33. Altıntig E, Yenigun M, Sari A, Altundag H, Tuzen M, Saleh TA (2021) Facile synthesis of zinc oxide nanoparticles loaded activated carbon as an eco-friendly adsorbent for ultra-removal of malachite green from water. *Environ. Technol. Innovation* 21:101305–101319. <https://doi.org/10.1016/j.eti.2020.101305>
34. Hassan AF, Mustafa AA, Esmail G, Awad AM (2022) Adsorption and photo-fenton degradation of methylene blue using nanomagnetite/potassium carrageenan bio-composite beads. *Arab J Sci Eng.* <https://doi.org/10.1007/s13369-022-07075-y>
35. Shaltout WA, El-Naggar GA, Esmail G, Hassan AF (2022) Synthesis and characterization of ferric@nanocellulose/nanohydroxyapatite bio-composite based on sea scallop shells and cotton stalks: adsorption of Safranin-O dye. *Biomass Convers Biorefinery.* <https://doi.org/10.1007/s13399-022-02753-1>
36. Langmuir I (1918) The adsorption of gases on plane surfaces of glass, mica and platinum. *J Am Chem Soc* 40:1361–1403. <https://doi.org/10.1021/ja02242a004>
37. Teodoro FS, Elias MMC, Ferreira GMD, Adarme OFH, Savedra RML, Siqueira MF, da Silva LHM, Gil LF, Gurgel LVA (2018) Synthesis and application of a new carboxylated cellulose derivative. Part III: Removal of auramine-O and safranin-T from mono- and bi-component spiked aqueous solutions. *J. Colloid Interface Sci.* 512:575–590. <https://doi.org/10.1016/j.jcis.2017.10.083>
38. Ghori SW, Rao GS (2021) Mechanical and thermal properties of date palm/kenaf fiber-reinforced epoxy hybrid composites. *Polym Compos* 42:2217–2224. <https://doi.org/10.1002/pc.25971>
39. Kumar A (2020) Sol gel synthesis of zinc oxide nanoparticles and their application as nano-composite electrode material for supercapacitor. *J Mol Struct* 1220:128654. <https://doi.org/10.1016/j.molstruc.2020.128654>
40. Moharram AH, Mansour SA, Hussein MA, Rashad M (2014) Direct precipitation and characterization of ZnO nanoparticles. *J Nanomater* 2014 <https://doi.org/10.1155/2014/716210>
41. Lonkar SP, Pillai V, Abdala A (2019) Solvent-free synthesis of ZnO-graphene nanocomposite with superior photocatalytic activity. *Appl Surf Sci* 465:1107–1113. <https://doi.org/10.1016/j.apsusc.2018.09.264>
42. Ramya V, Murugan D, Lajapathirai C, Sivasamy A (2018) Activated carbon (prepared from secondary sludge biomass) supported semiconductor zinc oxide nanocomposite photocatalyst for reduction of Cr(VI) under visible light irradiation. *J Environ Chem Eng* 6:7327–7337. <https://doi.org/10.1016/j.jece.2018.08.055>
43. Montalvo Andia J, Larrea A, Salcedo J, Reyes J, Lopez L, Yokoyama L (2020) Synthesis and characterization of chemically activated carbon from Passiflora ligularis, Inga feuillee and native plants of South America. *J Environ Chem Eng* 8:103892. <https://doi.org/10.1016/j.jece.2020.103892>
44. Yun SI, Kim SH, Kim DW, Kim YA, Kim B-H (2019) Facile preparation and capacitive properties of low-cost carbon nanofibers with ZnO derived from lignin and pitch as supercapacitor electrodes. *Carbon N Y* 149:637–645. <https://doi.org/10.1016/j.carbon.2019.04.105>
45. Gomez-Eerrano V, Valenzuela-Calahorro C, Pastor-Villegas J (1993) Characterization of rockrose wood and activated carbon. *Biomass Bioenergy* 4(5):35S364. [https://doi.org/10.1016/0961-9534\(93\)90052-6](https://doi.org/10.1016/0961-9534(93)90052-6)
46. Akpomie KG, Ghosh S, Gryzenhout M, Conradie J (2021) One-pot synthesis of zinc oxide nanoparticles via chemical precipitation for bromophenol blue adsorption and the antifungal activity against filamentous fungi. *Sci Rep* 11:1–17. <https://doi.org/10.1038/s41598-021-87819-2>
47. Hassan HS, Abol-Fotouh D, Salama E, Elkady MF (2022) Assessment of antimicrobial, cytotoxicity, and antiviral impact of a green zinc oxide/activated carbon nanocomposite. *Sci Rep* 12:1–12. <https://doi.org/10.1038/s41598-022-12648-w>
48. Zheng Y, Wu B (2021) Preparation process and characterization of activated carbon from mango kernels. *J Phys Conf Ser.* <https://doi.org/10.1088/1742-6596/2021/1/012061>
49. Umamaheswari A, Prabu SL, John SA, Puratchikody A (2021) Green synthesis of zinc oxide nanoparticles using leaf extracts of Raphanus sativus var. Longipinnatus and evaluation of their anticancer property in A549 cell lines. *Biotechnol Reports* 29:e00595. <https://doi.org/10.1016/j.btre.2021.e00595>
50. Nourmoradi H, Ghiasvand AR, Noorimotlagh Z (2015) Removal of methylene blue and acid orange 7 from aqueous solutions by activated carbon coated with zinc oxide (ZnO) nanoparticles: equilibrium, kinetic, and thermodynamic study. *Desalin Water Treat* 55:252–262. <https://doi.org/10.1080/19443994.2014.914449>
51. Vu DL, Seo JS, Lee HY, Lee JW (2017) Activated carbon with hierarchical micro-mesoporous structure obtained from rice husk and its application for lithium-sulfur batteries. *RSC Adv* 7:4144–4151. <https://doi.org/10.1039/C6RA26179E>
52. Lee WH, Rhee CK, Koo J, Lee J, Jang SP, Choi SUS, Lee KW, Bae HY, Lee GJ, Kim CK, Hong SW, Kwon Y, Kim D, Kim SH, Hwang KS, Kim HJ, Ha HJ, Lee SH, Choi CJ, Lee JH (2011) Round-robin test on thermal conductivity measurement of zno nanofluids and comparison of experimental results with theoretical bounds. *Nanoscale Res Lett* 6:258. <https://doi.org/10.1186/1556-276X-6-258>
53. Geed SR, Samal K, Tagade A (2019) Development of adsorption-biodegradation hybrid process for removal of methylene blue from wastewater. *J Environ Chem Eng* 7:103439. <https://doi.org/10.1016/j.jece.2019.103439>
54. Hassan AF, Elhadidy H (2017) Production of activated carbons from waste carpets and its application in methylene blue

- adsorption: Kinetic and thermodynamic studies. *J Environ Chem Eng* 5:955–963. <https://doi.org/10.1016/j.jece.2017.01.003>
55. Tan CHC, Sabar S, Hussin MH (2018) Development of immobilized microcrystalline cellulose as an effective adsorbent for methylene blue dye removal, South African. *J Chem Eng* 26:11–24. <https://doi.org/10.1016/j.sajce.2018.08.001>
  56. Başaran Kankılıç G, Metin AÜ (2020) *Phragmites australis* as a new cellulose source: Extraction, characterization and adsorption of methylene blue. *J Mol Liq* 312. <https://doi.org/10.1016/j.molliq.2020.113313>
  57. Hassan AF (2019) Synthesis of carbon nano-onion embedded metal–organic frameworks as an efficient adsorbent for cadmium ions: kinetic and thermodynamic studies. *Environ Sci Pollut Res* 26:24099–24111. <https://doi.org/10.1007/s11356-019-05581-5>
  58. Kamal KH, Dacrory S, Ali SSM, Ali KA, Kamel S (2019) Adsorption of Fe ions by modified carrageenan beads with tricarboxy cellulose: kinetics study and four isotherm models. *Desalin Water Treat* 165:281–289. <https://doi.org/10.5004/dwt.2019.24560>
  59. Mok CF, Ching YC, Osman NAA, Muhamad F, Hai ND, Choo JH, Hassan CR (2020) Adsorbents for removal of cationic dye: nanocellulose reinforced biopolymer composites. *J Polym Res* 27. <https://doi.org/10.1007/s10965-020-02347-3>
  60. Duman O, Polat TG, Diker CÖ, Tunç S (2020) Agar/ $\kappa$ -carrageenan composite hydrogel adsorbent for the removal of Methylene Blue from water. *Int J Biol Macromol* 160:823–835. <https://doi.org/10.1016/j.ijbiomac.2020.05.191>
  61. Üner O, Geçgel Ü, Bayrak Y (2016) Adsorption of methylene blue by an efficient activated carbon prepared from *Citrullus lanatus* rind: kinetic, isotherm, thermodynamic, and mechanism analysis. *Water Air Soil Pollut* 227(247). <https://doi.org/10.1007/s11270-016-2949-1>
  62. Vargas AM, Cazetta AL, Kunita MH, Silva TL, Almeida VC (2011) Adsorption of methylene blue on activated carbon produced from flamboyant pods (*Delonix regia*): study of adsorption isotherms and kinetic models. *Chem Eng J* 168:722–730. <https://doi.org/10.1016/j.cej.2011.01.067>
  63. Sangon S, Hunt AJ, Ngernyen Y, Youngme S, Supanchaiyamat N (2021) Rice straw-derived highly mesoporous carbon-zinc oxide nanocomposites as high performance photocatalytic adsorbents for toxic dyes. *J Clean Prod* 318:128583–128595. <https://doi.org/10.1016/j.jclepro.2021.128583>

**Publisher's note** Springer Nature remains neutral with regard to jurisdictional claims in published maps and institutional affiliations.

Springer Nature or its licensor (e.g. a society or other partner) holds exclusive rights to this article under a publishing agreement with the author(s) or other rightsholder(s); author self-archiving of the accepted manuscript version of this article is solely governed by the terms of such publishing agreement and applicable law.